Confined phase separation in SiO_X nanometric thin layers

Manuel Roussel, Etienne Talbot, Cristelle Pareige, R.P. Nalini, Fabrice Gourbilleau, Philippe Pareige

Confined phase separation in SiO_X nanometric thin layers

M. Roussel,[1] E. Talbot,[1,a)] C. Pareige,[1] R. Pratibha Nalini,[2] F. Gourbilleau,[2] and P. Pareige[1]
[1]*Groupe de Physique des Matériaux (GPM) UMR 6634, Normandie Université, Université et INSA de Rouen-CNRS, Av. de l'Université, BP 12, 76801 Saint Etienne du Rouvray, France*
[2]*Centre de Recherche sur les Ions, les Matériaux et la Photonique (CIMAP), CEA/CNRS/ENSICAEN/UCBN, 6 Bd. Maréchal Juin, 14050 Caen Cedex 4, France*

Phase separation in silicon-rich silica/silica multilayers was investigated using Atom Probe Tomography and Atomistic Kinetic Monte Carlo simulation. It is shown that the thickness of silicon-rich silicon oxide sublayers plays an important role during phase transformation. It determines the morphology of Si-rich phase formed after subsequent annealing, which is of prime interest for microelectronic and optoelectronic applications. Monte Carlo simulation reveals that the formation of isolated Si clusters can be achieved even in the case of spinodal decomposition and is directly related to the ratio between the spinodal wavelength and the sublayer thickness.

Because of its indirect band gap, silicon had never been considered for optoelectronic applications until 1990, when Canham showed that nanoporous silicon exhibits intense photoluminescence at room temperature.[1] Since this discovery, Si nanostructures have been intensively studied for their optical and electrical properties.[2] Among these structures, Si nanoparticles (Si-nps) embedded in silica (SiO_2) appears to be a promising system for optoelectronics and microelectronics and could be applied in future generations of solar cells,[3] waveguide amplifiers,[4] and non-volatile memories,[5] as it is suggested by hundreds of recent scientific articles. This enthusiasm is mainly due to the fact that Si-nps embedded in SiO_2 are easily obtained by phase separation between Si and SiO_2 in Si-rich silica (SiO_X) thin films during thermal annealing, which is fully compatible with the current silicon technology. In the meantime, many studies have demonstrated that the use of Si-nps requires an accurate control of the particle characteristics and the surrounding oxide quality.[1,6–8] Consequently, the formation mechanism of Si-nps in SiO_X is of prime interest, since it controls all the relevant parameters (shape of the Si-nps, diameter of the particles, interface with the surrounding oxide). Recently, it has been evidenced that phase separation mechanisms depend on Si supersaturation. At low Si excess, formation of Si-nps is initiated by nucleation reaction followed by growth regime[9,10] while at higher concentration interconnected Si-rich nanostructures formed by spinodal decomposition appear.[11,12] The limit between these two mechanisms is defined by the spinodal concentration limit which is close to 30% of Si excess in silica.[11,12] Finally, in both cases, at late stage (i.e., when the compositions of both phases have reached their equilibrium values), Ostwald ripening occurs.[13] Our investigation focuses more precisely on the phase separation in multilayered structures consisting of a successive stacking of SiO_X and SiO_2 sublayers. This kind of structure is commonly used in order to control Si-np size distribution[14] because the SiO_2 sublayers are supposed to act as diffusion barriers. It results in the formation of silicon nanoparticles having a diameter roughly equal to the thickness of the SiO_X sublayer. The goal of the present study is to understand the phase separation process occurring in such a confined thin film. For that purpose, Atom Probe Tomography (APT) was used in order to analyze various sets of multilayers systems and study the influence of SiO_X sublayer thickness. In addition, we have performed Atomistic Kinetic Monte Carlo (AKMC) simulations of phase separation in binary system in both bulk and thin film configurations. These simulations allow improving the fundamental understanding of the spinodal decomposition regime in thin SiO_X films and the resulting microstructure.

A set of SiO_X/SiO_2 multilayers (MLs) was deposited on [100] oriented silicon wafer using reactive radio frequency magnetron co-sputtering. Si and SiO_2 targets were used for SiO_X sublayers deposition under hydrogen-rich plasma while pure silicon oxide sublayers were deposited by sputtering pure silica target under Ar plasma. The MLs were grown at 500 °C with a power density of 2.2 and 7.4 $W \cdot cm^{-2}$ applied on the Si and SiO_2 targets, respectively. The sputtering time permitted to tune SiO_X and SiO_2 sublayer thicknesses. More details about the synthesis of SiO_X/SiO_2 MLs by magnetron sputtering can be found in Ref. 14. Two different sets of MLs were prepared. Sample A: SiO_X-4 nm/SiO_2-3 nm; Sample B: SiO_X-8 nm/SiO_2-10 nm. The silicon excess in SiO_X sublayers is the same in both set of samples and is measured to be 31%. Finally, to form Si-ncs, these samples have been submitted to various annealing treatments under N_2 atmosphere. Table I summarizes the different sets of multilayers and their respective annealing treatment.

APT experiments were performed using a Laser Assisted Wide Angle Tomographic Atom Probe (LAWATAP, CAMECA) using UV (343 nm) femto-second laser pulses (50 nJ, 350 fs). A full description of atom probe tomography technique can be found in Ref. 15, for example. Specimens for APT were prepared using a Dual-beam SEM-FIB NVision 40 (ZEISS) avoiding the incorporation of Ga^+ ions in the specimens during sample preparation. The details of the standard procedure are reported in previous works.[16,17] As it has been already demonstrated in previous works, APT

a)Electronic mail: etienne.talbot@univ-rouen.fr

TABLE I. Layer thicknesses and heat treatment for each multilayer.

Sample	SiO_X Thickness (nm)	SiO_2 Thickness (nm)	Annealing treatment Temperature-time
A_1	4	3	900 °C-15 min
A_2	4	3	900 °C-30 min
A_3	4	3	900 °C-1 h
A_4	4	3	900 °C-4 h
A_5	4	3	900 °C-8 h
A_6	4	3	900 °C-20 h
A_7	4	3	1000 °C-1 h
A_8	4	3	1100 °C-1 h
B_1	8	10	900 °C-1 h
B_2	8	10	1000 °C-1 h
B_3	8	10	1100 °C-1 h

is a powerful technique for giving a detailed microstructure at the atomic scale level of silicon nanoclusters in a SiO_2 host matrix.[10,18] Sample A was used to perform a complete kinetic study of the spinodal decomposition. Since it contains 31% of silicon excess, it is expected to decompose via a spinodal regime.[12] It was annealed at 900 °C for times ranging from 15 min up to 20 h (samples A_1–A_6). The corresponding APT reconstructions are presented in Fig. 1. As shown from Figs. 1(a)–1(e), a typical interconnected structure develops with ageing time. But the morphology changes after an annealing time of 20 h at 900 °C. Fig. 1(f) reveals isolated Si-nps. This microstructure may originate from two different phenomena which will be discussed in detail hereafter: (i) it can be the signature of a late stage coarsening regime. Indeed, the compositions of both phases have reached their equilibrium values. The major contribution to the driving force for unmixing in that case is the reduction of surface interphases between the two phases. Consequently, for a volume fraction lower than the percolation threshold, isolated particles are observed. (ii) It may stem from the confined characteristic of the thin layers in which the decomposition process takes place.

The influence of SiO_X sublayer thickness has been investigated by comparing the microstructure of two sets of sample containing −4 nm SiO_X sublayers (A_3, A_7, and A_8) and 8 nm SiO_X sublayers (B_1, B_2, and B_3) after an annealing treatment at 900 °C, 1000 °C, and 1100 °C during 1 h. Both samples (A_i and B_i) contain 31% of Si excess. APT results are presented in Fig. 2. In the case of 8 nm-thick SiO_X sublayers Figs. 2(a)–2(c), spinodal decomposition is indeed observed whatever the thermal budget. However, in the case of 4 nm-thick SiO_X sublayers, increasing the annealing time has a remarkable influence: the interconnected structure is no longer observed at 1000 °C and 1100 °C and isolated Si-nps have been formed Figs. 2(d)–2(f). These Si-nps have sharp interfaces and have a mean radius of 1.6 ± 0.1 nm. Once again, two assumptions can be proposed on the formation of Si-nps: (i) Increasing the annealing temperature leads to a change in decomposition mechanism (from spinodal decomposition at 900 °C to nucleation followed by growth at 1100 °C). Nevertheless, as it is reported in Ref. 12, due to the extremely low solubility limit of Si in SiO_2 and the Si-O phase diagram, one can expect that the spinodal concentration limit does not vary between 900 °C and 1100 °C.[19] (ii) Spinodal decomposition takes place in all samples and the formation of isolated Si-nps is due to the thickness of the SiO_X sublayer.

APT investigation strongly suggests an influence of the thickness of SiO_X sublayers on the decomposition process in the analysed systems. Nevertheless, a quantitative description of this phenomenon is still missing. For instance, we cannot predict a critical value for the thickness of SiO_X layers under which Si-nps will form. This is mainly due to the fact that a quantitative description of the spinodal decomposition is usually achieved by determining the decomposition wavelength using autocorrelation profiles.[20] In our case, the peculiar geometry of the sample and, more particularly, the thin layer thickness analyzed prevents such a measurement. In order to provide a better understanding of the phenomenon, we developed atomistic Atomistic Kinetic Monte Carlo simulations.

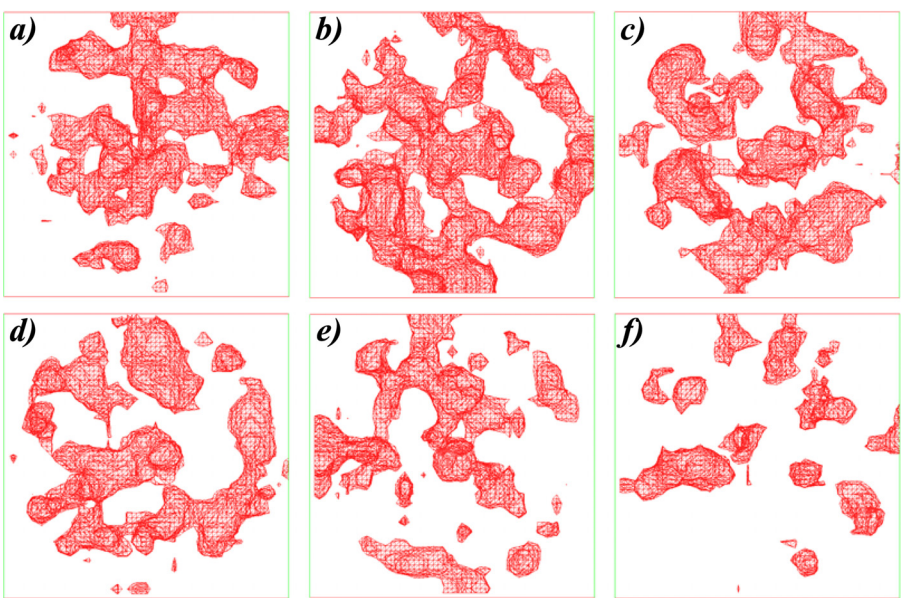

FIG. 1. Decomposition kinetics in SiO_X layers containing 31% of Si excess and annealed at 900 °C for: (a) 15 min (sample A_1); (b) 30 min (sample A_2); (c) 1 h (sample A_3); (d) 4 h (sample A_4); (e) 8 h (sample A_5); (f) 20 h (sample A_6). Si-rich phase is evidenced using 55 at. % of Si isoconcentration surfaces. Volumes: $12 \times 12 \times 4\,nm^3$.

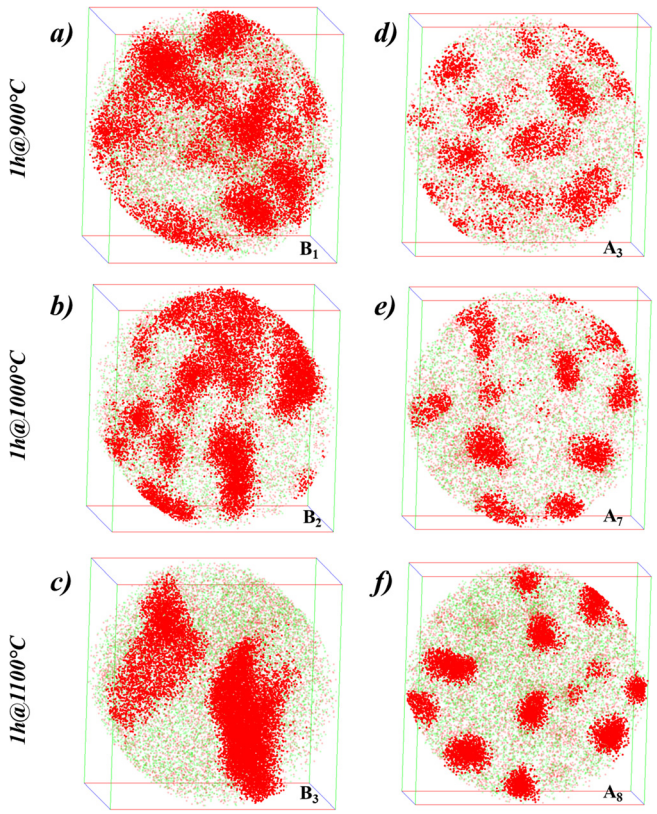

FIG. 2. Volume reconstructions of SiO_X sublayers for different annealing treatments and SiO_X sublayer thicknesses. (a)–(c) $SiO_X = 8$ nm; (d)–(f) $SiO_X = 4$ nm. Red dots correspond to silicon atoms and green ones correspond to oxygen atoms. Si-rich phase containing more than 55 at. % of Si atoms appears as bold red dots. Volumes: $12 \times 12 \times 8\,nm^3$ and $12 \times 12 \times 4\,nm^3$.

Muller *et al*. have used KMC to evidence a transition of phase separation mechanism from nucleation-growth to spinodal decomposition as a function of Si implantation doses in pure silica.[11,21] Besides, spinodal decomposition and phase separation have been theoretically or numerically investigated in constrained films.[22–24] Drawing inspiration from these works, we propose to combine our APT results with AKMC simulations in order to clarify the origin of the formation Si-nps through spinodal decomposition.

Modelling the kinetics of phase transformation between Si-rich and SiO_2 phases is a very complicated task because of the complexity of the system. To give just few major locks: non-isostructural structures of the two phases, ordered structure of SiO_2, amorphous structure of silica, and associated complex diffusion mechanisms in amorphous structure. Consequently, this accurate AKMC modelling does not exist, starting with a simplified model is a useful first step. As our goal was to study the evolution of spinodal decomposition confined in a nanometric layer and to get a reliable description of the kinetic of precipitation for confined thin layers, an AKMC model already developed to accurately simulate spinodal decomposition in binary AB alloy has been used.[20,25] Thus, the amorphous nature of the real material and diffusion mechanism which occurs in silica matrix have been neglected. The diffusion of atoms is based on thermally activated jumps of one vacancy towards one of its nearest neighbour atoms. The simulated crystals are constructed on a rigid BCC lattice. A and B atoms and one vacancy are distributed over $N = L^2 \times h$ cells. L corresponds to the planar dimension ($L = 64a_0$ with a_0 the lattice parameter of the BCC structure) while h corresponds to the thickness of the simulated layer. h varies between $8a_0$ and $64a_0$ (hereafter referred to as $8 \ldots 64$). Periodic boundary conditions are applied in the plane directions. Along the growth axis, boundaries act as walls in order to account for the presence of SiO_2 layers which play the role of diffusion barriers. Neither the vacancy nor the atoms can pass through these boundaries. The model relies on the residence time algorithm[26] to model the diffusion of the vacancy and is fully described in Refs. 20 and 25. As it has been explained before, one of the information that we cannot extract from APT analyses is the wavelength of the composition fluctuations, because of the peculiar geometry of the sample. AKMC simulations in the bulk case permit to overcome this problem. A reference simulation was performed in a bulk A-B system containing 30% of B species. It provided the B-rich phase fluctuation wavelengths for different simulation times in non-constrain case. AKMC simulations have been performed over 64^3 cells. In this case only, periodic boundary conditions were applied in the 3 spatial directions. The initial configuration of A and B species was chosen random. The 3D distributions of B atoms in the system aged for 0 Monte Carlo Steps (MCS) up to $10 \times 64 \times 10^8$ MCS are shown in Fig. 3. The measured wavelengths are reported in Table II. These values will permit to quantify the development of spinodal decomposition for each simulated time.

In order to clearly identify the influence of the thickness of the layer on the decomposition process, simulations were undertaken in thin layer configuration for the same alloy than in the previous case (i.e., 30% of B atoms). The simulated volume contained $L = 64^2$ cells in the plane of the layer while the thickness h varies from 4 to 16 cells.

Figure 4 shows the ageing evolution of the structure of B atoms as function of the thickness. (i) For the thickest layer ($h = 16$), ageing evolution is comparable to the bulk

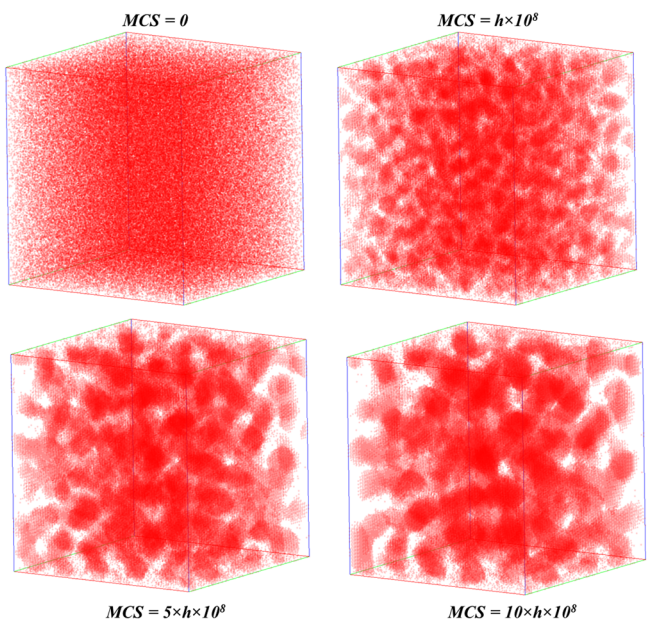

FIG. 3. AKMC simulation of spinodal decomposition in a bulk A-B system containing 30% of atom B, for different ageing times. Only B atoms are represented. The simulated volumes contain $64 \times 64 \times 64$ BCC cells.

TABLE II. Wavelength in the bulk case ($h = 64a_0$-periodic boundary conditions in all directions).

MCS	0	64×10^8	$5 \times 64 \times 10^8$	$10 \times 64 \times 10^8$
Wavelength (λ unit: a_0)	0	8.3	11.9	15.3

case. An interconnected structure developed during ageing. (ii) For the intermediate case ($h = 8$), we observe that after $MCS = 5 \times h \times 10^8$, the interconnected structure is lost to the benefit of B-pure isolated regions (B-nps). This effect is more pronounced at $MCS = 10 \times h \times 10^8$. It is worth to note that this kinetic reproduces the experimental one observed in sample A_2 to A_6 (Fig. 2). (iii) Concerning the thinnest layer ($h = 4$), B-pure isolated regions are observed since the first ageing times. No development of an interconnected microstructure is observed. These simulated kinetics reproduce remarkably well the experimental observations. To understand the behaviour of decomposition in a thin layer, we have compared the thickness of the layer with the fluctuation wavelength (estimated for the bulk). For the thickest layer, the thickness ($h = 16$) is always higher than the fluctuation wavelength which reaches $\lambda = 15.3a_0$. In this case as in the bulk case, an interconnected structure is still observed after $10 \times h \times 10^8 MCS$. It is important to note that, after this ageing time, no isolated particles that would be representative of the late stage of coarsening regime are observed.

For the intermediate case ($h = 8$), isolated B-nps appear when the wavelength becomes higher than the sublayer thickness. This phenomenon appears as soon as $MCS = 5 \times h \times 10^8$ (where $\lambda = 11.9$) and is even more pronounced for $MCS = 10 \times h \times 10^8$ (where $\lambda = 30.6$). As no late stage coarsening is expected after this ageing time as discussed above, the simulations show that the appearance of these isolated objects originates from the confinement in the thin layer. These results strongly suggest that the presence of

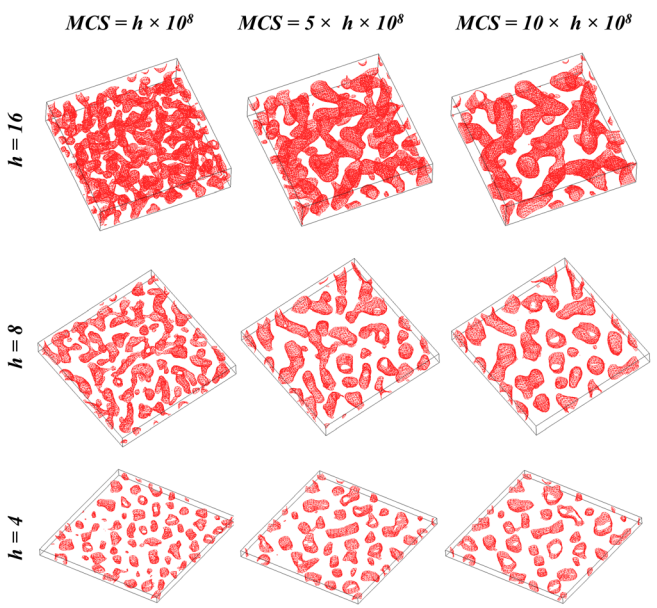

FIG. 4. AKMC simulation of spinodal decomposition in thin films for different ageing time. h indicates the thickness of the simulated layer. B-rich phase is evidenced using 55 at. % of B isoconcentration surfaces. Each simulated layer contains $64 \times 64 \times 64$ BCC cells.

the isolated Si-nps after 20 h of ageing at 900 °C in SiO_X sublayers containing 31% of excess Si (Fig. 2) is a size effect and not a kinetic effect (late stage of coarsening). It is clearly a consequence of the development of spinodal decomposition in a constrained layer. Finally, for the thinnest layer ($h = 4$), the wavelength is always higher than the thickness and B-nps are always observed. From these results and owing to the comparison of the ratio between bulk fluctuation wavelengths (Table II) and layer thicknesses for the different cases, one can conclude that isolated B-nps are present when $\lambda/h > 1$, which is in good agreement with phase field simulations performed by Seol *et al.*[22] This understanding of nanostructural changes in confined systems is of great importance for the development of high quality and performance of devices. In addition, besides the development needed to more accurately simulate these systems (on going work), this approach can easily be extended to other confined systems.

Owing to the fruitful comparison of APT experimental results and AKMC modelling, it has been evidenced that the formation of Si-nps can be achieved even in the range of spinodal decomposition regime. APT analyses evidenced that decreasing the thickness of the SiO_X sublayers in SiO_X/SiO_2 multilayered structures strongly influences the microstructure obtained after annealing. We demonstrated that after 1 h at 1000 °C or 1100 °C, in 8 nm-thick sublayers, interconnected and non-spherical Si-rich regions develop. For the same annealing treatment, in 4 nm-thick sublayers, isolated Si-nps are formed. This phenomenon is of prime interest, since the shape of silicon nanostructures directly influences the optical properties of such material. A simplified AKMC model has been used as a first step towards a better understanding of this phenomenon. It permitted to highlight the fact that isolated nanoparticles can be obtained by spinodal decomposition, provided that the wavelength is greater than the thickness of the layer.

This work was supported by the upper Normandy Research and the French Ministry of Research in the framework of Research Networks of Upper-Normandy. The authors also acknowledge "Le Fond Européen de Développement Régional" (FEDER) for its support. The simulations were performed at the "Centre de Ressources Informatiques de Haute Normandie" (CRIHAN) under Project No. 2005014.

[1] L. Canham, Appl. Phys. Lett. **57**, 1046 (1990).
[2] L. Pavesi and R. Turan, *Silicon Nanocrystals* (Wiley-VCH, 2010).
[3] F. Gourbilleau, C. Ternon, D. Maestre, O. Palais, and C. Dufour, J. Appl. Phys. **106**, 013501 (2009).
[4] M. Fujii, M. Yoshida, Y. Kanzawa, S. Hayashi, and K. Yamamoto, Appl. Phys. Lett. **71**, 1198 (1997).
[5] S. Tiwari, F. Rana, H. Hanafi, A. Harstein, E. Crabbe, and K. Chan, Appl. Phys. Lett. **68**, 1377 (1996).
[6] Y. Kanemitsu, Phys. Rev. B **53**, 13515 (1996).
[7] A. Romanyuk, V. Melnik, Y. Olikh, J. Biskupek, U. Kaiser, M. Feneberg, K. Thonke, and P. Oelhafen, J. Lumin. **130**, 87 (2010).
[8] P. Normand, E. Kapetanakis, P. Dimitrakis, D. Tsoukalas, K. Beltsios, N. Cherkashin, C. Bonafos, G. BenAssayag, H. Coffin, A. Claverie, V. Soncini, A. Agarwal, and M. Ameen, Appl. Phys. Lett. **83**, 168 (2003).
[9] L. A. Nesbit, Appl. Phys. Lett. **46**, 38 (1985).
[10] M. Roussel, E. Talbot, P. Pareige, and F. Gourbilleau, J. Appl. Phys. **113**, 063519 (2013).
[11] T. Muller, K. H. Heinig, and W. Möller, Appl. Phys. Lett. **81**, 3049 (2002).

[12]M. Roussel, E. Talbot, R. Prathiba-Nalini, F. Gourbilleau, and P. Pareige, Ultramicroscopy **132**, 290 (2013).
[13]C. Bonafos, B. Colombeau, A. Altibelli, M. Carrada, G. BenAssayag, B. Garrido, M. Lopez, A. Perez-Rodriguez, J. R. Morante, and A. Claverie, Nucl. Instrum. Methods Phys. Res. B **178**, 17 (2001).
[14]C. Ternon, F. Gourbilleau, X. Portier, P. Voivenel, and C. Dufour, Thin Solid Films **419**, 5 (2002).
[15]B. Gault, M. P. Moody, J. M. Cairney, and S. P. Ringer, *Atom Probe Microscopy* (Springer Verlag, Berlin, 2012).
[16]K. Thompson, D. Lawrence, D. J. Larson, J. D. Olson, T. F. Kelly, and B. Gorman, Ultramicroscopy **107**, 131 (2007).
[17]M. Roussel, E. Talbot, F. Gourbilleau, and P. Pareige, Nanoscale Res. Lett. **6**, 164 (2011).
[18]E. Talbot, R. Larde, F. Gourbilleau, C. Dufour, and P. Pareige, Europhys. Lett. **87**, 26004 (2009).
[19]S. M. Schnurre, J. Gröbner, and R. Schmidt-Fetzer, J. Non-Cryst. Solids **336**, 1 (2004).
[20]C. Pareige, M. Roussel, S. Novy, V. Kuksenko, P. Olsson, C. Domain, and P. Pareige, Acta Mater. **59**, 2404 (2011).
[21]T. Muller, K. H. Heinig, and W. Möller, Mater. Sci. Eng. B **101**, 49 (2003).
[22]D. J. Seol, S. Y. Hu, Y. L. Li, J. Shen, K. H. Oh, and L. Q. Chen, Acta Mater. **51**, 5173 (2003).
[23]S. M. Wise, J. S. Kim, and W. C. Johnson, Thin Solid Film **473**, 151 (2005).
[24]A. S. Abyzov and J. W. P. Schmelzer, J. Chem. Phys. **127**, 114504 (2007).
[25]C. Pareige, F. Soisson, G. Martin, and D. Blavette, Acta Mater. **47**, 1889 (1999).
[26]W. M. Young and E. W. Elcock, Proc. Phys. Soc. **89**, 735 (1966).